 doi:10.20944/preprints202204.0053.v1

Article

Computational Investigations on the Natural Small-Molecule as an Inhibitor of Programmed Death Ligand-1 for Cancer Immunotherapy

Geethu S Kumar [1, 2], Mahmoud Moustafa [3, 4], Amaresh Kumar Sahoo[5,*], Petr Malý[6,*], Shiv Bharadwaj [6,*]

[1] Department of Life Science, School of Basic Science and Research, Sharda University, Greater Noida, Uttar Pradesh, India
[2] Center for Bioinformatics, Computational and Systems Biology, Pathfinder Research and Training Foundation, Greater Noida, India
[3] Department of Biology, Faculty of Science, King Khalid University, Abha, Saudi Arabia
[4] Department of Botany and Microbiology, Faculty of Science, South Valley University, Qena, Egypt
[5] Department of Applied Sciences, Indian Institute of Information Technology Allahabad, Allahabad 211015, Uttar Pradesh, India
[6] Laboratory of Ligand Engineering, Institute of Biotechnology of the Czech Academy of Sciences v.v.i., BIOCEV Research Center, Vestec, Czech Republic
* **Corresponding authors:** AKS, Email: asahoo@iiita.ac.in**;** PM, Email: petr.maly@ibt.cas.cz **;**SB, Email: shiv.bharadwaj@ibt.cas.cz

Abstract: Several therapeutic monoclonal antibodies are approved by FDA against the PD-1/PD-L1 (programmed death-1/programmed death ligand-1) immune checkpoint, which has been a great success in cancer treatment. However, existing therapeutics, including small molecules inhibitors against PD-L1 checkpoint have certain drawbacks such as high cost and drug resistance that challenge the current available anti-PD-L1 therapy. Thereof, this study presents the screening of 32552 compounds from Natural Product Atlas database against PD-L1, including three steps of structure-based virtual screening and binding free energy refinement for the selection of potent PD-L1 inhibitors. Subsequently, five natural compounds, i.e., Neoenactin B1, Actinofuranone I, Cosmosporin, Ganocapenoid A, and 3-[3-hydroxy-4-(3-methylbut-2-enyl)phenyl]-5-(4-hydroxybenzyl)-4-methyl-dihydrofuran-2(3H)-one, were collected based on the ADMET (absorption, distribution, metabolism, excretion, and toxicity) profiling and binding free energy (>-70 kcal/mol) for further computational investigation by comparison to co-crystallised ligand, i.e. JQT inhibitor. Based on interaction mapping, explicit 100 ns molecular dynamics simulation, and post binding free energy calculations, all the compounds exhibited intermolecular interactions (hydrogen and hydrophobic) with essential residues and substantial complex stability by comparison to the JQT inhibitor. Collectively, the calculated results advocate the selected natural compounds as the putative potent inhibitors of PD-L1 and, therefore, can be considered for further development of PD-L1 immune checkpoint inhibitor in cancer immunotherapy.

Keywords: Programmed death ligand-1; Natural products; Immunotherapy; Neoenactin B1; Molecular dynamics simulation

1. Introduction

Cancer is a serious concern faced by researchers worldwide due to the increase in the number of patients and its capacity to shorten the human lifespan. International Agency for Research on Cancer (IARC) estimated ~19.3 million new cancer cases and almost 10 million cancer deaths in their Global Cancer Statistics (GLOBOCAN) 2020 report, in which one-half of the new cases and more than 58% of cancer deaths occurred in the Asian countries [1]. Although conventional treatment strategies, surgery, radiotherapies, and chemotherapy have shown massive progress in treating cancer within the past centuries, cancer patients, however, still endure problems during the treatment due to the low efficacy and

 doi:10.20944/preprints202204.0053.v1

side effects of the conventional therapeutics [2-4]. For example, multidrug resistance in cancer, which leads to the reduction in the efficacy rate of treatment and slows down the chances of getting a cure, has been linked with several mechanisms, including enhanced drug efflux, genetic mutations, certain growth factors, and an increase in the metabolic rate of xenobiotics [2]. Likewise, the efficacy of cancer radiotherapy, which mainly targets tumour cells and minimally damage normal cells, is based on the acceptable dose tolerance capacity of the adjacent normal cells and associated with post-therapy session side effects, such as skin peeling, blister formation, itching, fatigue, soreness, dry mouth, and even hair loss [5]. Thus, a profound understanding on the disease and drawbacks of the therapeutic strategies, an innovative approach, which mainly focuses on the specific target cells without damaging the adjacent healthy cells, is required for the cancer treatment [6].

In the tumour microenvironment, cancer cells power the activation of various immune checkpoint pathways that triggers immune suppression. Thus, cancer immunotherapy which aims to stimulate the immune system's ability to fight cancer is highly demanded in cancer treatment [7-9]. The advantage of this therapy is that it can prevent metastasis and recurrence of cancer cells along with treating primary cancer, marked as a standard treatment for cancer patients [10]. Programmed cell death-1 (PD-1, also known as CD279) T cell receptor and its ligands - programmed death ligand-1 (PD-L1 or B7-H1 or CD274) and programmed death ligand-2 (PD-L2 or B7-DC or CD273) - are the prime immune checkpoint pathway components, which are targeted for immune checkpoint inhibitory therapy against cancer [9,11].

Programmed death ligand-1 is a glycoprotein of 290 amino acids mainly expressed on the surface of cardiac endothelium, placenta, pancreatic isles, immune cells, epithelial cells, and tumour cells apart from T cells, B cells, and antigen-presenting cells (APC) [12-14]. The various cancer cells expressed PD-L1 and utilise the PD-1/PD-L1 pathway as an escape route from the T cell autoimmunity, to promote tumour growth [15]. For instance, the binding of PD-L1 to its receptor, i.e. PD-1, leads to suppression of T cell migration, proliferation, and secretion of cytokines, and hinders the ability to destroy tumor cells [16]. Thus, the various inhibitors of PD-1 and PD-L1, which can reverse the T cell suppression and enhance the anti-tumour immune response in the cancer patient have been reported [16,17]. For example, atezolizumab, avelumab, and durvalumab monoclonal antibodies (mAbs) are the FDA approved inhibitors, which target PD-L1 for the termination of tumour progression [16]. Although these therapeutics are highly effective and useful in cancer therapy but still have several shortcomings such as drug-resistance, durability, immunogenicity, high production costs, creating the need of introducing new molecules as potential inhibitors [18,19]. From this perspective, small-molecule based inhibitors are being researched to intervene the PD-1/PD-L1 signalling pathway in a fight against cancer, recently reviewed elsewhere [20,21].

Bioactive compounds derived from natural resources have been reported with anticancer properties by suppressing the gene expression responsible for tumour progression, making them easy to access and cost-effective [22]. For instance, S-Allylcysteine, an organo-sulphur, and Silibinin (a natural compound derived from *Silybum marianum* or milk thistle) are examples of natural compounds known to act as potential PD-L1 inhibitors [23,24]. Even though targeting the interface of PD-1/PD-L1 by small molecules inhibitors is challenging due to its 3D geometry, i.e., large and flat binding pockets, constant efforts have been added in the discovery of small molecules as PD-L1 inhibitors, reflected by the number of growing publications and patents [25,26]. However, none of the reported small molecules was able to progress into clinical trials so far [27]. Thus, finding natural products with the ability to inhibit the PD-L1 can lead to the development of a novel small molecule-based cancer immunotherapy. Besides, molecular docking simulations were recently applied to identify the potential terphenyl-based small-molecule inhibitors against PD-L1 to disturb the PD-1/PD-L1 pathway [27]. Thereof, in this study, we have applied the multi-step virtual screening protocol linked with binding free energy and

Preprints (www.preprints.org) | NOT PEER-REVIEWED | Posted: 7 April 2022 doi:10.20944/preprints202204.0053.v1

ADMET/pose filtering to identify the most putative natural compounds as PD-L1 inhibitors for cancer immunotherapy.

2. Methods

2.1. Receptor and ligand library collection

The three-dimensional (3D) crystal structure of the human programmed death ligand-1 (PD-L1) co-crystallized with (2~[16],4~[16])-1-[[5-chloranyl-2-[(3-cyanophenyl)methoxy]-4-[[3-(2,3-dihydro-1,4-benzodioxin-6-yl)-2-methyl-phenyl]methoxy]phenyl]methyl]-4-oxidanyl-

pyrrolidine-2-carboxylic acid (JQT) inhibitor at 2.20 Å resolution was retrieved as receptor from the RCSB Protein Data Bank (https://www.rcsb.org/; PBD ID: 6R3K) [27] Also, a total of 32552 natural compounds as ligand library was downloaded from the Natural Product Atlas database (https://www.npatlas.org/) [28] for multi-step structure-based virtual screening protocol against PD-L1 receptor.

2.2. Multi-step virtual screening and pose filtration

Multi-step virtual screening of the ligands against PD-L1 was performed using a virtual screening workflow in the Schrödinger suite-2020.4 [29]. Initially, the pre-processing of the PD-L1 receptor was using the PRIME tool [30,31] and protein preparation wizard [32] in the Schrödinger-maestro suite [29]. Briefly, the co-crystallised water molecules were removed from the receptor structure, which may obstruct the ligand interaction with the protein, while polar hydrogen atoms were added based on the hybridization of the carbon atoms, followed by protein structure refinement under default parameters using the Protein preparation wizard. Following, structure-based virtual screening, the key residues, viz. Phe[19], Ile[54], Tyr[56], Met[115], Ile[116], Ala[121], Asp[122], Tyr[123], Lys[124], and Arg[125] of Chain A and Tyr[56], Gln[66], Met[115], Ile[116], Ser[117], Ala[121], and Asp[122] of chain B in PD-L1 structure showing interactions with the co-crystalized ligand, i.e., JQT inhibitor, were considered for the docking grid generation using GLIDE v8.9 tool under default parameters in the Schrödinger suite-2020.4 [33].

Likewise, 32552 natural compounds as ligands were prepared under default parameters using LigPrep module tool in the Schrödinger-maestro suite [34]. Following, in the virtual screening workflow tool, all the ligands were filtered for ADME (absorption, distribution, metabolism, excretion) and drug-likeness criteria using the QikProp tool [35]. Later, the filtered ligands were virtually screened via three subsequent steps, including high throughput virtual screening (HTVS), standard precision (SP) screening and extra precision (XP) screening, where only 10% of the top screened ligands from the first step were considered in next successive step to collect the most potent ligands against the PD-L1 receptor. Finally, the post-process binding free energy calculations based on molecular mechanics generalised Born surface area (MM/GBSA) method was performed on the screened poses to collect the most suitable docking conformations of the ligands with the receptor for further computational analysis under default parameters with under OPLS (Optimized Potentials for Liquid Simulations)-3e force field in Prime MM/GBSA module of Maestro-Schrödinger suite 2020.4 [29,31]. The binding free energy and the additional energy components associated with the respective docked complexes were depicted via various steps using the mathematical equations (1-3).

$$\Delta G_{Bind} = \Delta G_{Com} - (\Delta G_{Rec} + \Delta G_{Lig}) = \Delta H - T\Delta S \approx \Delta E_{MM} + \Delta G_{sol} - T\Delta S \quad \ldots (1)$$

$$\Delta E_{MM} = \Delta E_{Int} + \Delta E_{Ele} + \Delta E_{vdW} \ldots (2)$$

$$\Delta G_{Sol} = \Delta G_{Pol} + \Delta E_{Nonpol} \ldots (3)$$

In the above-mentioned equations, $\Delta G_{Bind,}$ and ΔG_{Com} denote the binding free energy or Gibbs free energy and the total free energy of a docked complex containing protein and ligand, respectively. The sum of the protein and ligand in their free state is denoted by the $\Delta G_{Rec} + \Delta G_{Lig}$. The ΔG_{Bind} can also be computed from enthalpy (ΔH) and entropy ($-T\Delta S$)

 doi:10.20944/preprints202204.0053.v1

for the whole system under consideration using the second law of thermodynamics (Eq. 1). Here, in this study, the entropy contributing to the net ΔG_{Bind} was not calculated for the protein-ligand complexes due to the unavailability of expensive computational calculations. In addition, the entropy seems to have a low contribution to the net ΔG_{Bind} as reported earlier [36]. Therefore, ΔG_{Bind} of the protein-ligand complex is designated equivalent to *ΔH only and expressed as the sum of solvation free* (ΔG_{Sol}) *and molecular mechanical* (ΔE_{MM}) energy (Eq. 2). Usually, ΔE_{MM} constitutes the intermolecular, electrostatic, and van der Waals interactions energies represented as ΔE_{Int} , ΔE_{Ele} , and ΔE_{vdW}, respectively whereas the ΔG_{Sol} constitutes polar and non-polar energy represented as ΔG_{Pol} and $\Delta E_{Non-pol}$, respectively for the whole system. Hence, the ΔG_{Bind} for each docked protein-ligand complex was calculated using Prime MM/GBSA module under default parameters using the Prime MM/GBSA module of Maestro-Schrödinger suite 2020.4, as reported earlier [37,38].

Moreover, the crystal structure of PD-L1 with JQT inhibitor in the protein crystal structure was also docked in the protein pocket under similar conditions and used as a reference complex for the comparative analysis with the docked complexes of PD-L1 with screened natural compounds. The intermolecular analysis of the docked complexes was conducted under default parameters of the Maestro-Schrodinger package at 4 Å around the ligand in the binding pocket of the protein. All the 2D and 3D images of both the ligands and receptor were rendered in the free academic version of Maestro v12.6 tool of Schrödinger suite-2020.4 [39].

2.3. Molecular dynamic simulation

The selected best-docked poses were studied for the stability and intermolecular interaction as a function of 100 ns time under explicit classical molecular dynamics (MD) simulation on Linux environment over HP Z2 Microtower workstation using the free academic version of Desmond v5.6 [40] module in Maestro-Schrödinger suite 2018–4 [41]. Herein, each complex was placed in the centre of the orthorhombic grid box (10Å × 10Å × 10Å) solvated with TIP4P (transferable intermolecular potential 4 points) to collect maximum solvation effects of the natural solvent. Additionally, the whole system was neutralised using the counter sodium and chlorine ions while placed at 20 Å around the docked ligand within the binding pocket of the receptor. Moreover, 0.15 M salt was added to the system to mimic the physiological conditions for the docked complex using the system building tool. Furthermore, the complete system was subjected to 2000 steps and 1.0 kcal/mol/Å convergence threshold for the initial minimization using minimization tool. Eventually, the unrestrained 100 ns MD simulation trajectories were generated for each complex under a normal temperature and pressure (NPT) ensemble at 300K with a 10 ps step size under default parameters with Optimized Potentials for Liquid Simulations (OPLS)-2005 force field and later produced trajectories were analysed using the simulation interaction diagram (SID) tool in free academic Desmond v5.6 module with Maestro-Schrödinger suite 2018–4 interface [41].

2.4. End-point binding free energy calculation

The end-point binding free energy calculations were conducted on the last 10 ns interval of the 100 MD simulation for the selected complexes under the OPLS-3e force field using the Prime MM/GBSA module [29,31], as described earlier under section, 'Multi-step virtual screening and pose filtration'. Herein, extracted snapshots were treated for the removal of explicit solvent and ions molecules and computed net binding free energy is represented as mean with standard error.

Preprints (www.preprints.org) | NOT PEER-REVIEWED | Posted: 7 April 2022 doi:10.20944/preprints202204.0053.v1

3. Result and discussion

3.1. Virtual screening and ADMET analysis

The virtual screening techniques are commonly used in the drug discovery pipelines to identify the ligands with considerable binding affinity with receptor from the large compound databases. In this study, from the 173403 generated conformations for the 32552 natural compounds using Ligprep tool processed through drug-likeness filters, three levels of screening, i.e., HTVS, SP and XP, and MM/GBSA binding free energy calculations, resulting in an assortment of total 17 natural compounds against PD-L1 receptor. The collected natural compounds showed considerable ADMET properties, docking scores (> -10 kcal/mol) and binding free energy (> -40 kcal/mol) against the selected pocket of the PD-L1 receptor (**Table 1, S1**). Thus, based on the highest binding free energy values, the top five docked poses of PD-L1 with natural compounds, i.e., Neoenactin B1, Actinofuranone I, Cosmosporin A, Ganocapenoid A, and 3-[3-hydroxy-4-(3-methylbut-2-enyl)phenyl]-5-(4-hydroxybenzyl)-4-methyldihydrofuran-2(3H)-one, marked for high potency were selected for further intermolecular interaction analysis (**Fig. 1**). Of note, Neoenactin B1 was isolated as the antifungal compound from *Streptomyces olivoreticuli* [42] while Actinofuranone I, isolated from *Streptomyces gramineus*, was reported for anti-inflammatory property [43]. Likewise, isolation of Cosmosporin A, Ganocapenoid A, and 3-[3-hydroxy-4-(3-methylbut-2-enyl)phenyl]-5-(4-hydroxybenzyl)-4-methyldihydrofuran-2(3H)-one from the fungus *Pseudocosmospora* [44], *Ganoderma capense* [45], and *Aspergillus terreus* [46], respectively are not yet reported for any biological activity.

Table 1. Names and characteristics of the small molecules collected by screening process against the PD-L1 receptor from NP-Atlas database.

10	Title	Name	Mol. formula	Mol. Wt	Origin	Docking score (kcal/mol)	ΔG_{Bind} (kcal/mol)
1	NPA020827	Neoenactin B1	$C_{20}H_{38}N_2O_5$	386.531	*Streptomyces olivoreticuli subsp. Neoenacticus*	-10.36	-79.63
2	NPA027965	Actinofuranone I	$C_{23}H_{36}O_7$	424.533	*Streptomyces gramineus*	-10.92	-74.44
3	NPA026024	Cosmosporin A	$C_{22}H_{34}O_4$	362.508	*Pseudocosmospora sp. Bm-1-1*	-10.28	-67.30
4	NPA026082	Ganocapenoid A	$C_{21}H_{28}O_6$	376.449	*Ganoderma capense*	-10.54	-66.92
5	NPA013736	3-[3-hydroxy-4-(3-methylbut-2-enyl)phenyl]-5-(4-hydroxybenzyl)-4-methyldihydrofuran-2(3H)-one	$C_{23}H_{26}O_4$	366.456	*Aspergillus terreus*	-10.49	-64.74
6	NPA030364	4-carbglyceryl-3,3'-dihydroxy-5,5'-dimethyldiphenyl ether	$C_{18}H_{20}O_7$	348.352	*Aspergillus versicolor SCSIO 41502*	-10.45	-60.21
7	NPA004673	Not named	$C_{19}H_{16}O_3$	292.334	*Burkholderia pseudomallei*	-10.50	-57.08
8	NPA020009	Sterin A	$C_{16}H_{20}O_6$	308.33	*Stereum hirsutum*	-11.39	-55.39
9	NPA027779	Decarboxyunguidepside A	$C_{19}H_{20}O_5$	328.364	*Aspergillus unguis*	-10.39	-54.51
10	NPA025743	Premacrophorintriol-I	$C_{22}H_{34}O_5$	378.508	*Trichoderma sp. 1212-03*	-10.34	-54.42
11	NPA002619	4''-Deoxy-5'-Desmethyl-Terphenyllin	$C_{19}H_{16}O_4$	308.333	*Aspergillus sp. YXf3*	-10.56	-54.41
12	NPA018153	Linieodolide A	$C_{17}H_{30}O_6$	330.42	*Bacillus sp. 09ID194*	-10.30	-53.94
13	NPA017629	5'-O-desmethylterphenyllin	$C_{19}H_{16}O_5$	324.332	*Aspergillus sp. YXf3*	-10.62	-53.87
14	NPA011065	Nocarbenzoxazole E	$C_{16}H_{14}N_2O_5$	314.297	*Nocardiopsis lucentensis DSM 44048*	-10.73	-53.37
15	NPA022801	Floricolin Q	$C_{18}H_{14}O_5$	310.306	*Floricola striata*	-10.81	-52.11
16	NPA015571	Cylindrocarpol	$C_{23}H_{34}O_5$	390.519	*Acremonium sp.*	-11.86	-49.25
17	NPA014938	Baciphelacin	$C_{22}H_{34}N_2O_6$	422.52	*Bacillus thiaminolyticus IFO 3967/B-1-7*	-10.89	-40.41
18	JQT inhibitor	BDBM363278	$C_{36}H_{33}ClN_2O_7$	641.1	*Synthetic*	-9.824	-63.98

Preprints (www.preprints.org) | NOT PEER-REVIEWED | Posted: 7 April 2022 doi:10.20944/preprints202204.0053.v1

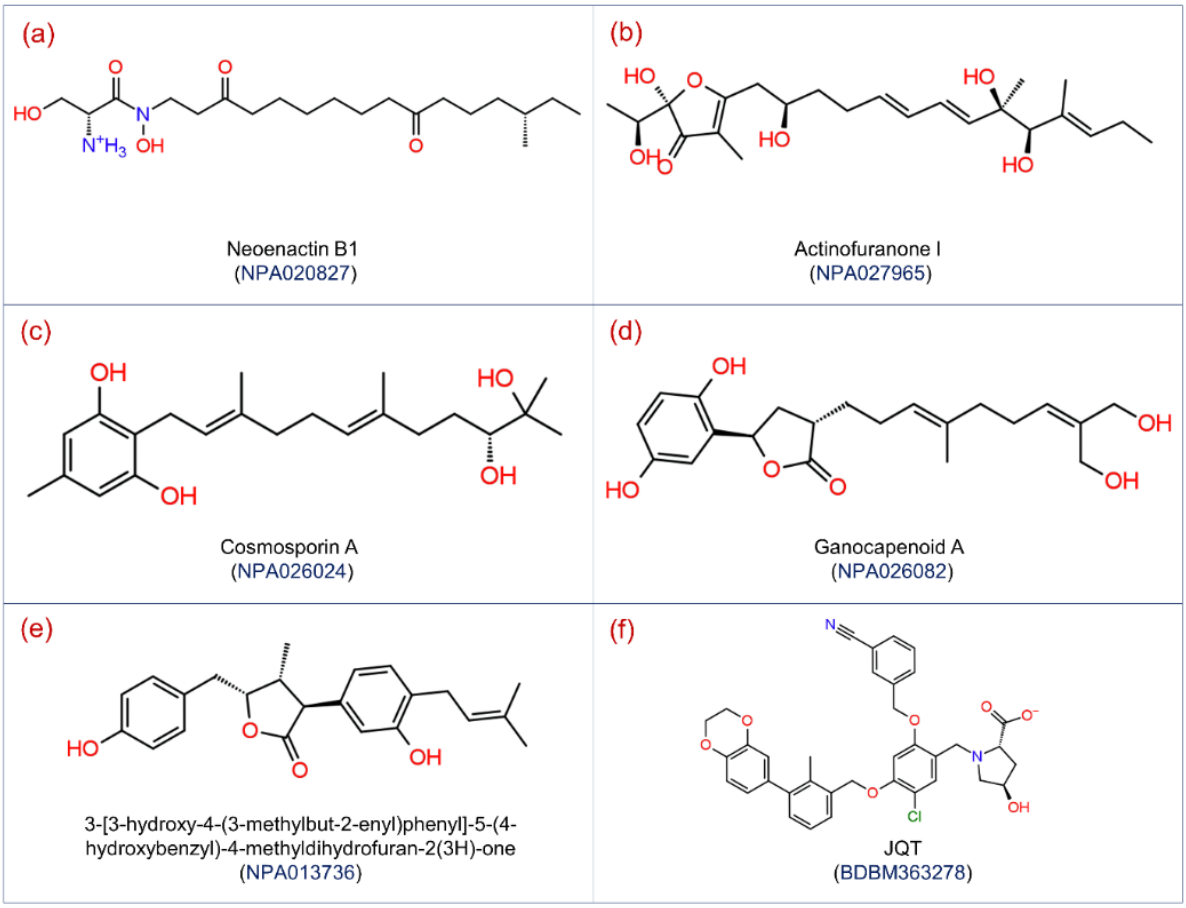

Figure 1. 2D structures of selected natural compounds, i.e., (a) Neoenactin B1, (b) Actinofuranone I, (c) Cosmosporin A, (d) Ganocapenoid A, (e) 3-[3-hydroxy-4-(3-methylbut-2-enyl)phenyl]-5-(4-hydroxybenzyl)-4-methyldihydrofuran-2(3H)-one, and (f) JQT inhibitor as the reference ligand, selected for the computational analysis against the PD-L1 receptor.

3.2. Molecular contact analysis

The molecular interaction analysis for the protein-ligand docked complex is employed to determine the effectiveness of the compound against a target in the structure-based drug discovery approaches [47]. Thus, molecular docked poses of the selected five natural compounds, i.e., Neoenactin B1, Actinofuranone I, Cosmosporin A, Ganocapenoid A, and 3-[3-hydroxy-4-(3-methylbut-2-enyl)phenyl]-5-(4-hydroxybenzyl)-4-methyldihydrofuran-2(3H)-one as putative inhibitors and JQT inhibitor as the reference ligand were studied for the residual interactions at 4 Å radius around the ligand in the docked pocket of the PD-L1 receptor (**Table 2**).

Preprints (www.preprints.org) | NOT PEER-REVIEWED | Posted: 7 April 2022 doi:10.20944/preprints202204.0053.v1

Table 2. Intermolecular interaction profiles for the docked natural compounds conformation with residues in the binding pocket of the PD-L1 receptor.

S.No.	Complex	H-bond	Hydrophobic	Polar	π-π/ *π-cation	Salt bridge	Positive	Negative
1	PD-L1- Neoenactin B1	A:Tyr^{123}, A:Lys^{124}, B:Tyr^{56}, B:Asp^{61}(2)	A:Ile^{54}, A:Tyr^{56}, A:Met^{115}, A:Ile^{116}, A:Ala^{121}, A:Tyr^{123}, B:Ile^{54}, B:Tyr^{56}, B:Met^{115}, B:Ile^{116}, B:Ala^{121}, B:Tyr^{123}	A:Ser^{117}, B:Asn^{63}, B:Gln^{66}, B:Ser^{117}	--	B:Asp^{61}	A:Lys^{124}, B:Lys^{62}	A:Asp^{122}, B:Glu^{58}, B:Asp^{61}, B:Asp^{122}
2	PD-L1- Actinofuranone I	A:Asp^{122}, B:Tyr^{56}, B:Asn^{63}	A: Ala^{18}, A:Phe^{19}, A:Ile^{54}, A:Val^{55}, A:Tyr^{56}, A:Met^{115}, A:Ile^{116}, A:Ala^{121}, A:Tyr^{123}, B:Ile^{54}, B:Tyr^{56}, B:Val^{68}, B:Val^{76}, B:Met^{115}, B:Ile^{116}, B:Ala^{121}, B:Tyr^{123}	A:Thr^{20}, A:Gln^{66}, A:Ser^{117}, B:Asn^{63}, B:Ser^{117}	--	--	A: Lys^{124}	A:Asp^{122}, B:Asp^{122}
3	PD-L1- Cosmosporin A	A:Asp^{122}, A:Tyr^{123}, A:Lys^{124}, B:Asp^{122}	A:Ile^{54}, A:Tyr^{56}, A:Met^{115}, A: Ile^{116}, A:Ala^{121}, A:Tyr^{123}, B: Ile^{54}, B:Tyr^{56}, B:Met^{115}, B:Ile^{116}, B:Ala^{121}, B:Tyr^{123}	A:Ser^{117}, B:Gln^{66} B:Ser^{117}	--	--	A:Lys^{124},	A:Asp^{122}, B: Asp^{61} B:Asp^{122}
4	PD-L1- Ganocapenoid A	A:Ala^{121}, B:Ala^{121}	A:Ile^{54}, A:Tyr^{56}, A:Val^{68}, A:Met^{115}, A:Ile^{116}, A: Ala^{121}, A:Tyr^{123}, B:Ile^{54}, B:Tyr^{56}, B:Val^{68}, B:Met^{115}, B:Ile^{116}, B:Ala^{121}, B:Tyr^{123}	A: Gln^{66}, A: Ser^{117}, B: Gln^{66}, B: Ser^{117}	A:Tyr^{56}	--	--	A:Asp^{122}, B:Asp^{122}
5	PD-L1-3-[3-hydroxy-4-(3-methylbut-2-enyl)phenyl]-5-(4-hydroxybenzyl)-4-methyldihydrofuran-2(3H)-one	B:Ala^{122}, B:Met^{115}	A:Ile^{54}, A:Tyr^{56}, A:Met^{115}, A:Ile^{116}, A:Ala^{121}, A:Tyr^{123}, B:Ile^{54}, B:Val^{55}, B:Tyr^{56}, B:Met^{115}, B:Ile^{116}, B:Ala^{121}, B:Tyr^{123}	A: Gln^{66}, A: Ser^{117}, B: Gln^{66}, B: Ser^{117}	A:Tyr^{56}	--	B:Lys^{124}	A:Asp^{122}, B:Asp^{122}
6	PD-L1-JQT inhibitor	--	A:Ala^{18}, A:Phe^{19} , A:Ile^{54} ,A:Val^{55}, A:Tyr^{56} , A:Met^{115}, A:Ile^{116}, A:Ala^{121} A:Tyr^{123}, B:Ile^{54}, B:Tyr^{56} , B:Val^{68} , B:Met^{115}, B:Ile^{116}, B:Ala^{121}, B:Tyr^{123}	A:Thr^{20}, A:Gln^{66}, A:Ser^{117}, B:Asn^{63}, B:Gln^{66}, B:Ser^{117}	A:Lys^{124}, B:Tyr^{56}, *A:Lys^{124}	A:Lys^{124}	A:Lys^{124,} A:Arg^{125}	A:Asp^{122}, B:Asp^{61}, B:Asp^{122s}

The analysis of docked PD-L1-Neoenactin B1 complex shows five hydrogen bonds (H-bonds) formation with A:Tyr^{123}, A:Lys^{124}, B:Tyr^{56}, and B:Asp^{61}(2) residues; PD-L1-Actinofuranone I complex also showed three H-bonds with A:Asp^{122}, B:Tyr^{56}, and B:Asn^{63} residues; PD-L1-Cosmosporin A complex exhibits four H-bonds with A:Asp^{122}, A:Tyr^{123}, A:Lys^{124}, and B:Asp^{122} residues; PD-L1-Ganocapenoid A complex depicts two H-bonds interaction with A:Ala^{121} and B:Ala^{121} residues; and PD-L1-3-[3-hydroxy-4-(3-methylbut-2-enyl)phenyl]-5-(4-hydroxybenzyl)-4-methyldihydrofuran-2(3H)-one complex shows formation of two H-bonds with B:Ala^{122} and B:Met^{115} residues (**Table 2, Fig. 2, S1**). However, no H-bond formation was observed in the reference complex, i.e., PD-L1-JQT inhibitor (**Table 2, Fig. 2, S1**). Also, only PD-L1-Neoenactin B1 complex was noted for salt-bridge formation with B:Asp^{61} residue by comparison to PD-L1-JQT inhibitor complex (A:Lys^{124}). Moreover, PD-L1-Ganocapenoid A and PD-L1-3-[3-hydroxy-4-(3-methylbut-2-enyl)phenyl]-5-(4-hydroxybenzyl)-4-methyl dihydrofuran-2(3H)-one complexes exhibited π-π stacking interactions at A:Tyr^{56} residue by comparison to PD-L1-JQT inhibitor complex, which showed both π-π (B:Tyr^{56}) and π-cation stacking interactions (A:Lys^{124}). Additionally, docked natural compounds in the binding pocket of PD-L1 were also observed for other residual interactions, involving hydrophobic, polar, positive, and negative interactions (**Table 2, Fig. 2, S1)**. Notably, interacting residues with the natural compounds were also noted in the interaction map of reference complex, indicating the natural compounds have relatively occupied the same binding pocket as the reference ligand. Thereof, based on the binding energy profiles (docking scores and binding free energy) in association with observed intermolecular interactions of the docked natural compounds against JQT inhibitor with PD-L1 receptor, predicted the substantial stability of the natural compounds in the binding pocket of PD-L1 by comparison to JQT inhibitor, and may contribute to inhibition of the PD-1/PD-L1 pathway, as reported for JQT inhibitor [27].

Preprints (www.preprints.org) | NOT PEER-REVIEWED | Posted: 7 April 2022 doi:10.20944/preprints202204.0053.v1

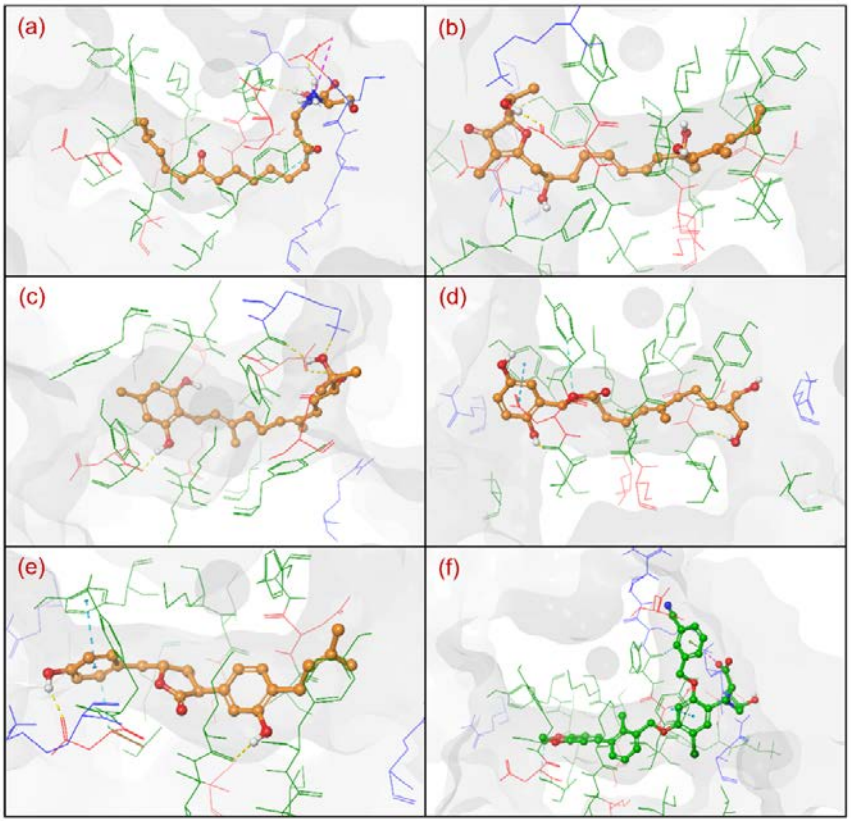

Figure 2. 3D poses of the selective natural compounds, i.e., (a) Neoenactin B1, (b) Actinofuranone I, (c) Cosmosporin A, (d) Ganocapenoid A, (e) PD-L1-3-[3-hydroxy-4-(3-methylbut-2-enyl)phenyl]-5-(4-hydroxybenzyl)-4-methyldihydrofuran-2(3H)-one, (f) JQT inhibitor as the reference compound screened against the binding pocket of PD-L1 collected at 4 Å space around the ligand within in the docked site of PDL-1 protein.

3.3. Molecular dynamic simulation analysis

To predict the dynamic stability and intermolecular interactions as a function of 100 ns, classical MD simulation was performed on each docked PD-L1-natural compound, viz. Neoenactin B1, Actinofuranone I, Cosmosporin A, Ganocapenoid A, and 3-[3-hydroxy-4-(3-methylbut-2-enyl)phenyl]-5-(4-hydroxybenzyl)-4-methyldihydrofuran-2(3H)-one complex and analyzed by comparison to the apo-PD-L1 receptor and reference docked complex, i.e., PD-L1-JQT inhibitor, simulation trajectories.

Initially, the last poses of the 100 ns MD simulations were recovered and compared with respective docked poses for molecular contacts and conformational changes in both protein and ligand (**Table S2, Fig. 3, S2-3**). Notably, all the last poses of the docked natural compounds with PD-L1 receptor after 100 ns MD simulation were observed for consistent residual interactions by comparison to the respective docked poses, supporting the stability of all the docked natural compounds in the binding pocket of PD-L1 receptor by comparison to the reference complex (**Table S2, Fig. S2**). Moreover, 3D surface analysis of the last poses from the 100 ns MD simulation reveals substantial conformational changes in the protein structure docked with natural compounds against JQT inhibitor, predicting the potential of docked natural compounds to significantly disturb the native conformational of the protein (**Fig. 3, S3**). Furthermore, the MD simulation trajectories of the respective docked complexes were statically analysed in terms of root mean square deviation (RMSD), root mean square fluctuation (RMSF), and protein-ligand interactions mapping to understand the dynamic stability of the docked complexes as a function of 100 ns MD simulation interval.

Preprints (www.preprints.org) | NOT PEER-REVIEWED | Posted: 7 April 2022 doi:10.20944/preprints202204.0053.v1

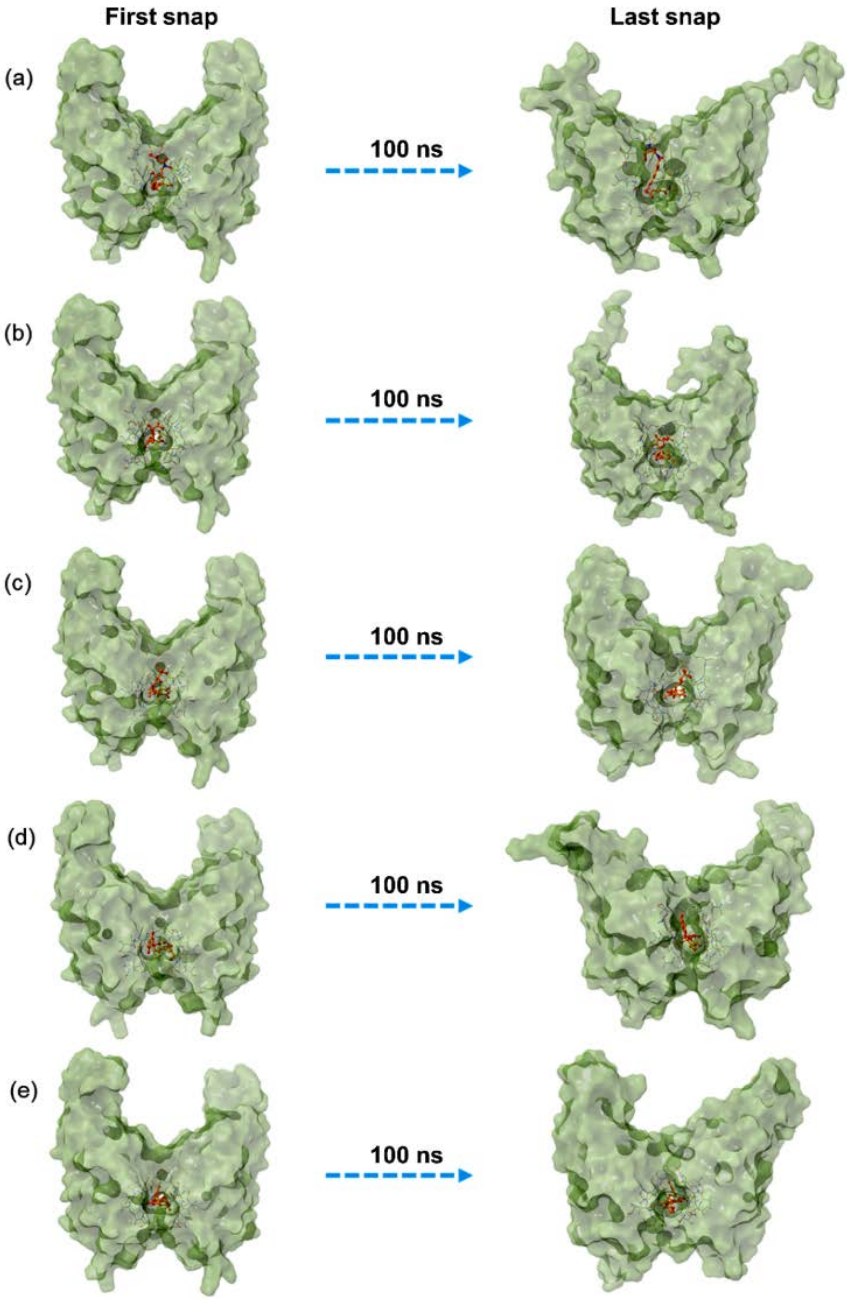

Figure 3. Representation of the 3D conformational changes in the last poses, i.e., (a) PD-L1-Neoenactin B1, (b) PD-L1-Actinofuranone I, (c) PD-L1-Cosmosporin A, (d) PD-L1-Ganocapenoid A, (e) PD-L1-3-[3-hydroxy-4-(3-methylbut-2-enyl)phenyl]-5-(4-hydroxybenzyl)-4-methyldihydrofuran-2(3H)-one, logged from 100 ns MD simulation trajectory by comparison to the respective docked poses. .

3.4. RMSD and RMSF analysis

Initially, RMSD values were computed from the respective docked poses of PD-L1-natural compounds as a function of 100 ns simulation interval and analyzed by comparison to the RMSD values of apo-protein and PD-L1-JQT inhibitor complex (**Fig. 4, S5**). In all the docked complexes of PD-L1 with natural compounds, substantial deviations (> 3.5 Å) were observed in the receptor throughout 100 ns MD simulation, except in PD-L1-Ganocapenoid A complex where equilibrium in the protein RMSD (~ 4 Å) was noted after 40 ns till the end of the 100 ns MD simulation while PD-L1 receptor exhibited higher deviations (> 4.8 Å) in PD-L1-Neoenactin B1 and PD-L1-Actinofuranone I docked complexes during the course of simulation. However, PD-L1 docked with JQT inhibitor showed high deviation (~ 4 Å) within the first 10 ns interval followed by a state of global

Preprints (www.preprints.org) | NOT PEER-REVIEWED | Posted: 7 April 2022 doi:10.20944/preprints202204.0053.v1

minima (~ 3 Å) till the end of simulation while apo-PD-L1 receptor was also noted for consistent deviations (< 4.2 Å) on several occasions without a state of equilibrium during MD simulation interval. These observations suggested that, unlike JQT inhibitors, docked natural compounds, particularly Neoenactin B1 and Actinofuranone I, may promote the strong global conformational changes in the PD-L1 receptor. These observations were further supported by the calculated RMSF values (> 2.5 Å) for the docked PD-L1 with Neoenactin B1 and Actinofuranone I natural compounds by comparison to apo-protein (< 2.5 Å) and protein docked with JQT inhibitor (< 2.5 Å) (**Fig. S4-S5**).

Likewise, protein-fit ligand RMSD analysis indicated substantial global minima (< 3 Å) for all the docked natural compounds, except Cosmosporin A and 3-[3-hydroxy-4-(3-methylbut-2-enyl)phenyl]-5-(4-hydroxybenzyl)-4-methyldihydrofuran-2(3H)-one (< 2 Å) as observed for the JQT inhibitor (< 2 Å), throughout the 100 ns MD simulation interval (**Fig. 4**). Moreover, computed ligand RMSF also reveals the acceptable values (< 3 Å) for all the docked natural compounds with PD-L1 against the JQT inhibitor, suggesting the substantial stability of the docked ligand with the protein (**Fig. S6**). Collectively, RMSD and RMSF analysis of the docked complexes suggested the considerable stability of the docked ligands with the protein while docked natural compounds may induce substantial conformational changes in the protein structure that results in the inhibition of PD-L1 protein with its receptor in the PD-1/PL-1 pathway.

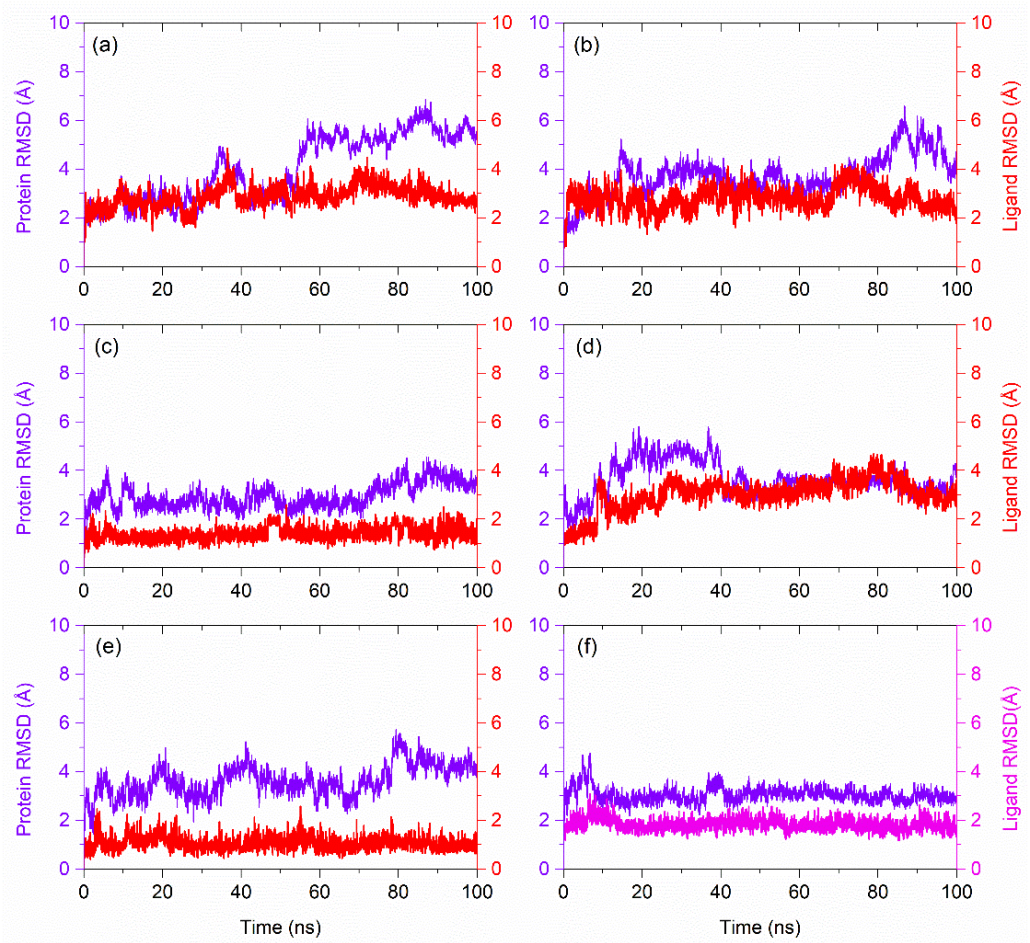

Figure 4. RMSD plots for the PD-L1-natural compounds, i.e., (a) Neoenactin B1, (b) Actinofuranone I, (c) Cosmosporin A, (d) Ganocapenoid A, (e) 3-[3-hydroxy-4-(3-methylbut-2-enyl)phenyl]-5-(4-hydroxybenzyl)-4-methyldihydrofuran-2(3H)-one, and (f) PD-L1-JQT inhibitor complexes as function of 100 ns simulation interval. Herein, protein RMSD values were extracted in terms of alpha carbon atoms while ligand RMSD values were computed as the protein-fit ligand for all the docked complexes from their respective 100 ns MD simulation trajectories.

 doi:10.20944/preprints202204.0053.v1

3.5. Protein-Ligand Interaction mapping

To further access the stability of the docked complexes in terms of intermolecular interactions as a function of simulation interval, protein-ligand contact maps, including hydrogen bonding, hydrophobic interactions, ionic interactions, and water bridge formation, were extracted from the respective MD simulation trajectories (**Fig. 5, S7).** Notably, all the docked natural compounds showed considerable molecular contacts with the active residues in the binding pocket of the PD-L1 during the 100 ns MD simulation interval by comparison to the reference complex, i.e., PD-L1-JQT inhibitor; the interacting residues were also noted in the initially docked poses (**Table 2**).

In the PDL1-Neoenactin B1 complex, B:Asp^{61} exhibits hydrogen bond formation for 100% of the simulation time while B:Tyr^{56} and A:Tyr^{123} residues were noted for hydrophobic interactions with docked ligand for 20% of the total simulation time. Also, B:Glu^{58} residue showed 50% and 15% of total interaction fractions in water bridge formation and ionic bond formations during the 100 ns simulation interval (**Fig. 5)**. Likewise, in the PDL1-Actinofuranone I complex, A:Asp^{122} residue contributed in 90% of the interaction fraction for H-bond formation, in addition to water bridge interaction (60%) during the total simulation interval. Moreover, A:Tyr^{56} and A:Tyr^{123} residues showed 30% of the interaction fraction in hydrophobic interactions, A:Arg^{125} exhibited 50% of the interaction fraction in water bridge formation, and B:Tyr^{56} formed 70% of the interaction fraction in H-bonding during the 100 ns MD simulation (**Fig. 5)**. Also, protein-ligand contact analysis of PDL1-Cosmosporin A showed substantial contribution of A:Tyr^{56}, B:Tyr^{56}, and B:Ala^{121} residues in hydrophobic interaction (50% interaction fraction); A:Tyr^{123} (90% interaction fraction) and B:Asp^{122} (85% interaction fraction) residues in H-bond formation, and A:Arg^{125} residue (55% interaction fraction) in water bridge formation during 100 ns MD simulation interval (**Fig. 5)**. Furthermore, analysis of PDL1- Ganocapenoid A complex showed substantial contribution of A:Tyr^{56} residue (65% interaction fraction) and A:Gln^{66} (55% interaction fraction) in hydrogen bond formation; B:Asp^{73} (55% interaction fraction) residue exhibits water bridge formation, and B:Tyr^{123} (85% interaction fraction) in the hydrophobic interactions during the 100 ns simulation interval (**Fig. 5)**. Whilst, analysis of protein-ligand mapping of PDL1-3-[3-hydroxy-4-(3-methylbut-2-enyl)phenyl]-5-(4-hydroxybenzyl)-4-methyldihydrofuran-2(3H)-one complex shows A:Tyr^{56} and B: Tyr^{56} hydrophobic interaction for 70% of interaction fraction; B:Tyr^{123} (45% interaction fraction) forms a hydrophobic interaction; B:Met^{115} (45% interaction fraction) in H-bonding, and B: Asp^{122} (40% interaction fraction) in water bridge formation during 100 ns MD simulation interval (**Fig. 5**). Whereas the protein-ligand mapping of the PD-L1 protein with its native ligand JQT inhibitor exhibits ionic interaction via A:Asp^{122} residue (45% interaction fraction), hydrophobic interaction via B:Tyr^{56} residue (100% interaction fraction), hydrophobic interaction via A:Tyr^{123} residue (80% interaction fraction), H-bond formation via A:Arg^{125} (80% interaction fraction), and water bridge formation via A:Lys^{124} residue (20% interaction fraction) during 100 ns MD simulation (**Fig. S7**). Additionally, molecular contact formation between the receptor and docked natural compounds were also logged at 30% of the total simulation interval, indicated substantial contribution of H-bonding and hydrophobic interactions by comparison to the reference complex (**Fig. S7-S8**). Altogether, collected interaction profiles as a function of simulation interval indicating a substantial contribution of H-bonds and hydrophobic interactions in the dynamic stability of PD-L1-natural compounds complexes during the 100 ns MD simulation. Hence, based on 100 ns MD simulation analysis, the selected docked complexes can be arranged in order of stability, i.e., PDL1-Neoenactin B1, PDL1-Cosmosporin A, PDL1-Actinofuranone I, PDL1-Ganocapenoid A, and PDL1-3-[3-hydroxy-4-(3-methylbut-2-enyl)phenyl]-5-(4 hydroxybenzyl)methyldihydrofuran an-2(3H)-one, by comparison to the reference complex, viz. PD-L1-JQT inhibitor.

Preprints (www.preprints.org) | NOT PEER-REVIEWED | Posted: 7 April 2022 doi:10.20944/preprints202204.0053.v1

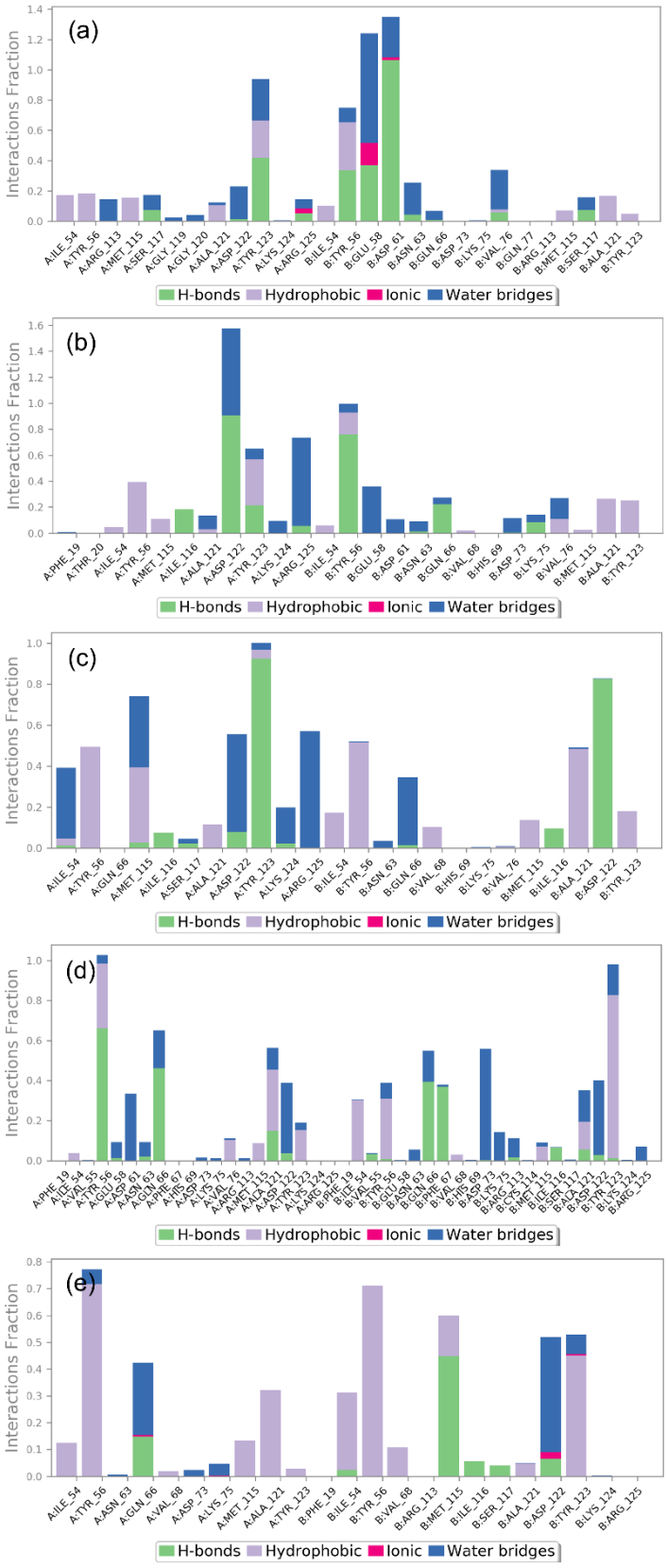

Figure 5. Protein-ligand interactions mapping PD-L1 and selected natural compounds, i.e., (a) Neoenactin B1, (b) Actinofuranone I, (c) Cosmosporin A, (d) Ganocapenoid A, and (e) 3-[3-hydroxy-4-(3-methylbut-2-enyl)phenyl]-5-(4-hydroxybenzyl)-4-methyldihydrofuran-2(3H)-one fit on protein were extracted from 100 ns MD simulation trajectories of respective docked complexes.

Preprints (www.preprints.org) | NOT PEER-REVIEWED | Posted: 7 April 2022 doi:10.20944/preprints202204.0053.v1

3.6. Binding free energy analysis

The binding affinities of the five selected protein-ligand complexes were estimated using MM/GBSA approach. Herein, poses of the PDL1-natural compound, i.e., Neoenactin B1, Actinofuranone I, Cosmosporin A, Ganocapenoid A, and 3-[3-hydroxy-4-(3-methylbut-2-enyl)phenyl]-5-(4 hydroxybenzyl)methyldihydrofuran-2(3H)-one, were retrieved from 100 ns MD simulation trajectory at every 10 ps from the last 10 ns interval of 100 ns MD simulation trajectory for the average calculation of binding free energy (ΔG_{Bind}) along with energy dissociation components against the reference complex (**Table S3, Fig. 6**).

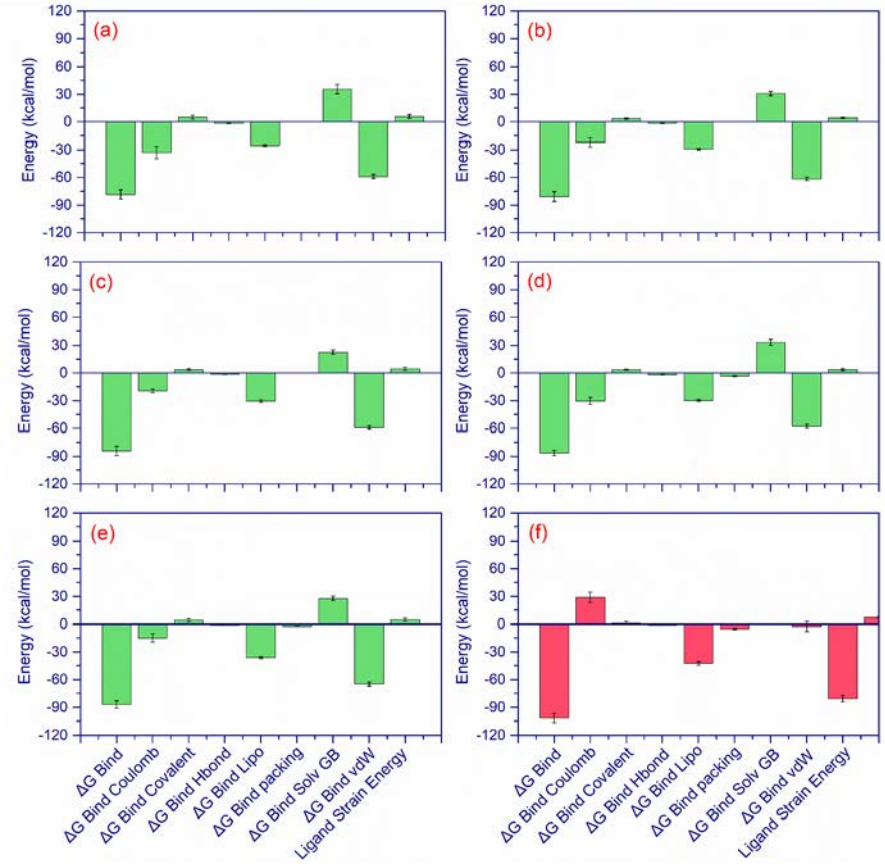

Figure 6. Binding free energy and individual dissociation energy components calculation performed for PDL1 and selected natural compounds, i.e., (a) Neoenactin B1 (b) Actinofuranone I (c) Cosmosporin A, (d) Ganocapenoid A (e) 3-[3-hydroxy-4-(3-methylbut-2-enyl)phenyl]-5-(4-hydroxybenzyl)-4-methyldihydrofuran-2(3H)-one (f) JQT inhibitor, reference compound.

All the docked complexes exhibit appropriate binding energy higher than -70 kcal/mol, where the highest binding free energy (-87.21 ± 4.11 kcal/mol) was obtained for the PD-L1-3-[3-hydroxy-4-(3-methylbut-2-enyl)phenyl]-5-(4hydroxybenzyl)methyldihydrofuran-2(3H)-one docked complex and lowest binding free energy was recorded in the PD-L1-Neoenactin B1 (-78.66 ± 5.02 kcal/mol) complex by comparison to PD-L1-JQT inhibitor complex (-101.77 ± 4.94 kcal/mol) (**Fig. 6**). Whereas the binding energy of the docked complex PD-L1-Actinofuranone I was -80.91 ± 5.16 kcal/mol followed by -84.41 ± 5.08 kcal/mol for PD-L1-Cosmosporin A and -86.45 ± 2.81 kcal/mol for PD-L1-Ganocapenoid A (**Fig. 6**). Furthermore, the computation of dissociation energy components for each complex shows that $\Delta G_{Bind\ Lipo}$ (Lipophilic energy) and $\Delta G_{Bind\ vdW}$ (Van der Waals interaction energy) significantly added to the stability of docked complexes, whereas $\Delta G_{Bind\ Solv\ GB}$ (Generalized Born electrostatic solvation energy) substantially favoured to the instability of the respective docked complexes (**Table S3, Fig. 6**). From the analysis of calculated

binding free energy values, natural compounds are endorsed as potential hit candidates for the development of PD-L1 inhibitors for cancer immunotherapy.

4. Conclusion

Programmed death ligand-1 (PD-L1) is a potential target for the suppression of cancer progression. The development of anti-cancer compounds using natural compounds by inhibiting the PD-L1 protein can be a turning point in the field of cancer immunotherapy. In this study, five natural products, i.e., Neoenactin B1, Actinofuranone I, Cosmosporin A, Ganocapenoid A, and 3-[3-hydroxy-4-(3-methylbut-2-enyl)phenyl]-5-(4 hydroxybenzyl)methyldihydrofuran-2(3H)-one are identified as potential hits candidates with substantial docking energy (> -10 kcal/mol), MMGBSA energy (> -60 kcal//mol) and drug-likeness as putative ligands for the PD-L1 inhibition. Based on the intermolecular interaction profiling of the docked poses and 100 ns molecular dynamic simulation trajectory analysis promotes the substantial contribution of H-bonding and hydrophobic interactions in the stability of docked natural compounds with the PD-L1 receptor. Furthermore, calculated net binding free energy on each trajectory supports the stability of the docked complexes by comparison to reference ligand and advocated the selected compounds as potent hit candidates for the development of PD-L1 inhibitors. Overall, the computational investigation of the natural compounds as PD-L1 inhibitor provides a positive endorsement for the selected natural compounds in the eventual designing and development of an effective small molecule-based anti-PD-L1 agent, which can provide PD-L1 inhibition at low concentration, for the cancer immunotherapy.

Acknowledgments: Dr Mahmoud Moustafa thanks the Deanship of Scientific Research, King Khalid University, Saudi Arabia for funding this work under grant no. : R.G.P. -1/244/42. The authors also acknowledge the received technical support from Institute of Biotechnology CAS by the Institutional Research Concept (RVO: 86652036).

Author Contributions: Conceptualization: SB, AKS, and PM; Methodology: GSK and MM; Data curation and Formal analysis: GSK, and SB; Investigation: GSK, and AKS; Software: AKS; Validation and Visualization: AKS, SB and PM; Roles/Writing - original draft: GSK and SB ; Writing - review & editing: MM, SB, AKS and PM; Supervision: AKS, PM and SB.

Reference

1. Sung, H.; Ferlay, J.; Siegel, R.L.; Laversanne, M.; Soerjomataram, I.; Jemal, A.; Bray, F. Global Cancer Statistics 2020: GLOBOCAN Estimates of Incidence and Mortality Worldwide for 36 Cancers in 185 Countries. *CA: a cancer journal for clinicians* **2021**, *71*, 209-249, doi:10.3322/caac.21660.
2. Bukowski, K.; Kciuk, M.; Kontek, R. Mechanisms of Multidrug Resistance in Cancer Chemotherapy. *International journal of molecular sciences* **2020**, *21*, doi:10.3390/ijms21093233.
3. Wang, Y.; Wang, M.; Wu, H.X.; Xu, R.H. Advancing to the era of cancer immunotherapy. *Cancer communications* **2021**, *41*, 803-829, doi:10.1002/cac2.12178.
4. Wyld, L.; Audisio, R.A.; Poston, G.J. The evolution of cancer surgery and future perspectives. *Nature reviews. Clinical oncology* **2015**, *12*, 115-124, doi:10.1038/nrclinonc.2014.191.
5. Allen, C.; Her, S.; Jaffray, D.A. Radiotherapy for Cancer: Present and Future. *Advanced drug delivery reviews* **2017**, *109*, 1-2, doi:10.1016/j.addr.2017.01.004.
6. Tay, R.E.; Richardson, E.K.; Toh, H.C. Revisiting the role of CD4(+) T cells in cancer immunotherapy-new insights into old paradigms. *Cancer gene therapy* **2021**, *28*, 5-17, doi:10.1038/s41417-020-0183-x.
7. Khalil, D.N.; Smith, E.L.; Brentjens, R.J.; Wolchok, J.D. The future of cancer treatment: immunomodulation, CARs and combination immunotherapy. *Nature reviews. Clinical oncology* **2016**, *13*, 273-290, doi:10.1038/nrclinonc.2016.25.
8. Ribas, A.; Wolchok, J.D. Cancer immunotherapy using checkpoint blockade. *Science* **2018**, *359*, 1350-+, doi:10.1126/science.aar4060.
9. Sharma, P.; Allison, J.P. Dissecting the mechanisms of immune checkpoint therapy. *Nature reviews. Immunology* **2020**, *20*, 75-76, doi:10.1038/s41577-020-0275-8.
10. Park, W.; Heo, Y.J.; Han, D.K. New opportunities for nanoparticles in cancer immunotherapy. *Biomater Res* **2018**, *22*, 24, doi:10.1186/s40824-018-0133-y.
11. Hu, Z. Chapter 11 - Using CAR-NK cells to overcome the host resistance to antibody immunotherapy and immune checkpoint blockade therapy. In *Successes and Challenges of NK Immunotherapy*, Bonavida, B., Jewett, A., Eds.; Academic Press: 2021; pp. 193-212.
12. Chowdhury, P.S.; Chamoto, K.; Honjo, T. Combination therapy strategies for improving PD-1 blockade efficacy: a new era in cancer immunotherapy. *Journal of internal medicine* **2018**, *283*, 110-120, doi:10.1111/joim.12708.
13. Qin, W.; Hu, L.; Zhang, X.; Jiang, S.; Li, J.; Zhang, Z.; Wang, X. The Diverse Function of PD-1/PD-L Pathway Beyond Cancer. *Frontiers in immunology* **2019**, *10*, 2298, doi:10.3389/fimmu.2019.02298.

14. Salmaninejad, A.; Valilou, S.F.; Shabgah, A.G.; Aslani, S.; Alimardani, M.; Pasdar, A.; Sahebkar, A. PD-1/PD-L1 pathway: Basic biology and role in cancer immunotherapy. *Journal of cellular physiology* **2019**, *234*, 16824-16837, doi:10.1002/jcp.28358.
15. Muenst, S.; Soysal, S.D.; Tzankov, A.; Hoeller, S. The PD-1/PD-L1 pathway: biological background and clinical relevance of an emerging treatment target in immunotherapy. *Expert opinion on therapeutic targets* **2015**, *19*, 201-211, doi:10.1517/14728222.2014.980235.
16. Akinleye, A.; Rasool, Z. Immune checkpoint inhibitors of PD-L1 as cancer therapeutics. *Journal of hematology & oncology* **2019**, *12*, 92, doi:10.1186/s13045-019-0779-5.
17. Han, Y.; Liu, D.; Li, L. PD-1/PD-L1 pathway: current researches in cancer. *American journal of cancer research* **2020**, *10*, 727-742.
18. Li, K.; Tian, H. Development of small-molecule immune checkpoint inhibitors of PD-1/PD-L1 as a new therapeutic strategy for tumour immunotherapy. *Journal of drug targeting* **2019**, *27*, 244-256, doi:10.1080/1061186X.2018.1440400.
19. Zhan, M.M.; Hu, X.Q.; Liu, X.X.; Ruan, B.F.; Xu, J.; Liao, C. From monoclonal antibodies to small molecules: the development of inhibitors targeting the PD-1/PD-L1 pathway. *Drug discovery today* **2016**, *21*, 1027-1036, doi:10.1016/j.drudis.2016.04.011.
20. Wu, Q.; Jiang, L.; Li, S.C.; He, Q.J.; Yang, B.; Cao, J. Small molecule inhibitors targeting the PD-1/PD-L1 signaling pathway. *Acta Pharmacol Sin* **2021**, *42*, 1-9, doi:10.1038/s41401-020-0366-x.
21. Awadasseid, A.; Wu, Y.; Zhang, W. Advance investigation on synthetic small-molecule inhibitors targeting PD-1/PD-L1 signaling pathway. *Life Sci* **2021**, *282*, 119813, doi:10.1016/j.lfs.2021.119813.
22. Ri, M.H.; Ma, J.; Jin, X. Development of natural products for anti-PD-1/PD-L1 immunotherapy against cancer. *Journal of Ethnopharmacology* **2021**, *281*, 114370.
23. Khan, F.; Pandey, P.; Mishra, R.; Arif, M.; Kumar, A.; Jafri, A.; Mazumder, R. Elucidation of S-allylcysteine role in inducing apoptosis by inhibiting PD-L1 expression in human lung cancer cells. *Anti-Cancer Agents in Medicinal Chemistry (Formerly Current Medicinal Chemistry-Anti-Cancer Agents)* **2021**, *21*, 532-541.
24. Rugamba, A.; Kang, D.Y.; Sp, N.; Jo, E.S.; Lee, J.M.; Bae, S.W.; Jang, K.J. Silibinin Regulates Tumor Progression and Tumorsphere Formation by Suppressing PD-L1 Expression in Non-Small Cell Lung Cancer (NSCLC) Cells. *Cells* **2021**, *10*, doi:10.3390/cells10071632.
25. Zak, K.M.; Grudnik, P.; Guzik, K.; Zieba, B.J.; Musielak, B.; Domling, A.; Dubin, G.; Holak, T.A. Structural basis for small molecule targeting of the programmed death ligand 1 (PD-L1). *Oncotarget* **2016**, *7*, 30323-30335, doi:10.18632/oncotarget.8730.
26. Zak, K.M.; Kitel, R.; Przetocka, S.; Golik, P.; Guzik, K.; Musielak, B.; Domling, A.; Dubin, G.; Holak, T.A. Structure of the Complex of Human Programmed Death 1, PD-1, and Its Ligand PD-L1. *Structure* **2015**, *23*, 2341-2348, doi:10.1016/j.str.2015.09.010.
27. Muszak, D.; Surmiak, E.; Plewka, J.; Magiera-Mularz, K.; Kocik-Krol, J.; Musielak, B.; Sala, D.; Kitel, R.; Stec, M.; Weglarczyk, K.; et al. Terphenyl-Based Small-Molecule Inhibitors of Programmed Cell Death-1/Programmed Death-Ligand 1 Protein-Protein Interaction. *Journal of medicinal chemistry* **2021**, *64*, 11614-11636, doi:10.1021/acs.jmedchem.1c00957.
28. van Santen, J.A.; Poynton, E.F.; Iskakova, D.; McMann, E.; Alsup, Tyler A.; Clark, T.N.; Fergusson, C.H.; Fewer, D.P.; Hughes, A.H.; McCadden, C.A.; et al. The Natural Products Atlas 2.0: a database of microbially-derived natural products. *Nucleic Acids Research* **2021**, *50*, D1317-D1323, doi:10.1093/nar/gkab941.
29. Schrödinger Release 2020-4, **Schrödinger**, LLC, New York, NY, 2020.
30. Jacobson, M.P.; Pincus, D.L.; Rapp, C.S.; Day, T.J.; Honig, B.; Shaw, D.E.; Friesner, R.A. A hierarchical approach to all-atom protein loop prediction. *Proteins* **2004**, *55*, 351-367, doi:10.1002/prot.10613.
31. Schrödinger Release 2020-4: Prime, **Schrödinger**., LLC, New York, NY, 2020.
32. Sastry, G.M.; Adzhigirey, M.; Day, T.; Annabhimoju, R.; Sherman, W. Protein and ligand preparation: parameters, protocols, and influence on virtual screening enrichments. *J Comput Aided Mol Des* **2013**, *27*, 221-234, doi:10.1007/s10822-013-9644-8.
33. Schrödinger Release 2020-4: Glide, **Schrödinger**., LLC, New York, NY, 2020.
34. Schrödinger Release 2020-4: LigPrep, **Schrödinger**., LLC, New York, NY, 2020.
35. Schrödinger Release 2020-4: QikProp, **Schrödinger**., LLC, New York, NY, 2020.
36. Hou, T.; Wang, J.; Li, Y.; Wang, W. Assessing the performance of the MM/PBSA and MM/GBSA methods. 1. The accuracy of binding free energy calculations based on molecular dynamics simulations. *J Chem Inf Model* **2011**, *51*, 69-82, doi:10.1021/ci100275a.
37. Bharadwaj, S.; Dubey, A.; Yadava, U.; Mishra, S.K.; Kang, S.G.; Dwivedi, V.D. Exploration of natural compounds with anti-SARS-CoV-2 activity via inhibition of SARS-CoV-2 Mpro. *Brief Bioinform* **2021**, doi:10.1093/bib/bbaa382.
38. Mena-Ulecia, K.; Tiznado, W.; Caballero, J. Study of the Differential Activity of Thrombin Inhibitors Using Docking, QSAR, Molecular Dynamics, and MM-GBSA. *Plos One* **2015**, *10*, Doi:10.1371/journal.pone.0142774.
39. Schrödinger Release 2020-4: Maestro, **Schrödinger**., LLC, New York, NY, 2020.
40. Bowers, K.J.; Chow, E.; Xu, H.; Dror, R.O.; Eastwood, M.P.; Gregersen, B.A.; Klepeis, J.L.; Kolossvary, I.; Moraes, M.A.; Sacerdoti, F.D. Scalable algorithms for molecular dynamics simulations on commodity clusters. In Proceedings of the Proceedings of the 2006 ACM/IEEE conference on Supercomputing, 2006; p. 84.
41. Schrödinger Release 2018-4: Maestro, **Schrödinger**., LLC, New York, NY, 20218.
42. Roy, S.K.; Inouye, Y.; Nakamura, S.; Furukawa, J.; Okuda, S. Isolation, structural elucidation and biological properties of neoenactins B1, B2, M1 and M2, neoenactin congeners. *The Journal of antibiotics* **1987**, *40*, 266-274, doi:10.7164/antibiotics.40.266.
43. Ma, J.; Cao, B.; Liu, C.; Guan, P.; Mu, Y.; Jiang, Y.; Han, L.; Huang, X. Actinofuranones DI from a lichen-associated actinomycetes, streptomyces gramineus, and their anti-inflammatory effects. *Molecules* **2018**, *23*, 2393.
44. Nakamura, T.; Suzuki, T.; Ariefta, N.R.; Koseki, T.; Aboshi, T.; Murayama, T.; Widiyantoro, A.; Kurniatuhadi, R.; Malik, A.; Annas, S. Meroterpenoids produced by Pseudocosmospora sp. Bm-1-1 isolated from Acanthus ebracteatus Vahl. *Phytochemistry Letters* **2019**, *31*, 85-91.
45. Liao, G.-F.; Wu, Z.-H.; Liu, Y.; Yan, Y.-M.; Lu, R.-M.; Cheng, Y.-X. Ganocapenoids A–D: Four new aromatic meroterpenoids from Ganoderma capense. *Bioorganic & Medicinal Chemistry Letters* **2019**, *29*, 143-147.
46. Awaad, A.S.; Nabilah, A.J.A.; Zain, M.E. New antifungal compounds from Aspergillus terreus isolated from desert soil. *Phytotherapy Research* **2012**, *26*, 1872-1877.
47. Bharadwaj, S.; Lee, K.E.; Dwivedi, V.D.; Yadava, U.; Kang, S.G. Computational aided mechanistic understanding of Camellia sinensis bioactive compounds against co-chaperone p23 as potential anticancer agent. *Journal of Cellular Biochemistry* **2019**, *120*, 19064-19075.